Journal of Catalysis 275 (2010) 108–116

Contents lists available at ScienceDirect

Journal of Catalysis

journal homepage: www.elsevier.com/locate/jcat

Au on $MgAl_2O_4$ spinels: The effect of support surface properties in glycerol oxidation

Alberto Villa [a], Aureliano Gaiassi [a], Ilenia Rossetti [b], Claudia L. Bianchi [b], Klaus van Benthem [c,1], Gabriel M. Veith [d,*], Laura Prati [a,**]

[a] Dipartimento di Chimica Inorganica, Metallorganica e Analitica L.Malatesta, Università degli Studi di Milano, via Venezian 21 – 20133 Milano, Italy
[b] Dipartimento di Chimica Fisica e Elettrochimica, Università degli Sudi di Milano, via Golgi 19 – 20133 Milano, Italy
[c] Dept. Chemical Engineering & Materials Science, University of California, Davis, 3098 Bainer Hall, 1 Shields Ave., Davis, CA 95616, United States
[d] Materials Science and Technology Division, Oak Ridge National Laboratory, Oak Ridge, TN 37831, United States

ARTICLE INFO

Article history:
Received 28 June 2010
Revised 21 July 2010
Accepted 22 July 2010
Available online 21 August 2010

Keywords:
Gold catalyst
Spinel structure
Glycerol oxidation

ABSTRACT

Here, we investigated the properties of Au nanoparticles prepared via three different techniques and supported on three different $MgAl_2O_4$ spinels. After careful characterization of bare and gold-loaded supports (XPS, BET, XRD, STEM) and catalytic test for the selective oxidation of glycerol, we concluded that the surface composition and area of the spinel play an important role in determining the selectivity of the catalyst as well as gold particle size. When supported on surface characterized by a similar Al/Mg ratio, gold clusters selectivity is not mediated by particle dimension. For example, large gold particles on $MgAl_2O_4$, which typically produce high selectivity to glycerate when supported on aluminum-rich surfaces instead, enhance the C–C bond cleavage reaction. Accordingly, the selectivity of similarly sized AuNPs on $MgAl_2O_4$ spinels with the same surface Al/Mg ratio is similar but we demonstrate that the activity depends on gold surface exposure (at.% Au by XPS) and on support surface area.

1. Introduction

Gold nanoparticles (AuNPs) have attracted attention since ancient times for their beautiful color, but recently there has been increasing interest in gold NPs for different applications, in particular as catalysts [1–3]. Indeed, supported or non-supported AuNPs are catalytically active in many reactions, including CO oxidation, water–gas shift reaction, propylene epoxidation and acetylene hydrochlorination [4–6]. Arguably, one of the potential applications of AuNPs is the catalytic oxidation of alcohols to carbonyl compounds or carboxylic acids, which are valuable organic synthesis precursors [7–11]. While colloidal or colloid-like systems have shown catalytic activity for the liquid-phase oxidation of alcohols [12–15], supported AuNPs are far more investigated for alcohol oxidations as they are easier to handle and recover. Glycerol is an intriguing starting reagent since it is a major co-product of biodiesel production. Its conversion into valuable products is of upmost importance for biomass valorization and it can be considered a polyfunctional material, which is very useful as a feedstock for fine chemical synthesis. Glycerol transformations have been well studied, with the oxidative transformation one of the most investigated [16–18]. Catalysts normally suffer from deactivation mainly ascribed to the irreversible adsorption of reaction products that, especially in the case of glycerol, have strong chelating properties (Scheme 1) due to the co-presence of OH and COOH functional groups. The selective oxidation of glycerol is normally carried out in aqueous solution under mild conditions (50–60 °C, 3–10 bar O_2) and in the presence of a base that prolongs the catalyst life [7,9,11,19–26]. Recently, gold-catalyzed selective glycerol oxidation has been performed with H_2O_2 as the oxidant, resulting in a different set of products' distributions (glycolic acid as main product) [27] (Scheme 1).

A suitable support material is crucial for catalytic activity as well as for catalyst stability. The brutal conditions present in liquid-phase reactions lead to more stringent requirements for the choice of support material and catalyst chemistry to maintain activity and selectivity. While one of the main roles of the support is to avoid coalescence and agglomeration of the AuNPs by reducing their mobility, metal-support interaction can also play an important role in the reaction mechanism. Nanoparticles supported on reducible oxides such as TiO_2 and CeO_2, where the transition metal ion exists in two different oxidation states and vacancy chemistry plays a role in catalytic mechanisms, are classic examples of support-induced properties of the catalyst [2,10].

The $MgAl_2O_4$ spinel is a widely used refractory material due to its high melting temperature (2135 °C) and thermal stability [28]. These properties combined with its hydrothermal stability make it a promising catalyst support for applications such as

* Corresponding author. Fax: +39 02503 14405.
** Corresponding author.
E-mail addresses: Laura.Prati@unimi.it (G.M. Veith), veithgm@ornl.gov (L. Prati).
[1] Previously at the Center for Nanophase Materials Sciences, Oak Ridge National Laboratory, Oak Ridge, TN 37831, United States.

0021-9517/$ - see front matter © 2010 Elsevier Inc. All rights reserved.
doi:10.1016/j.jcat.2010.07.022

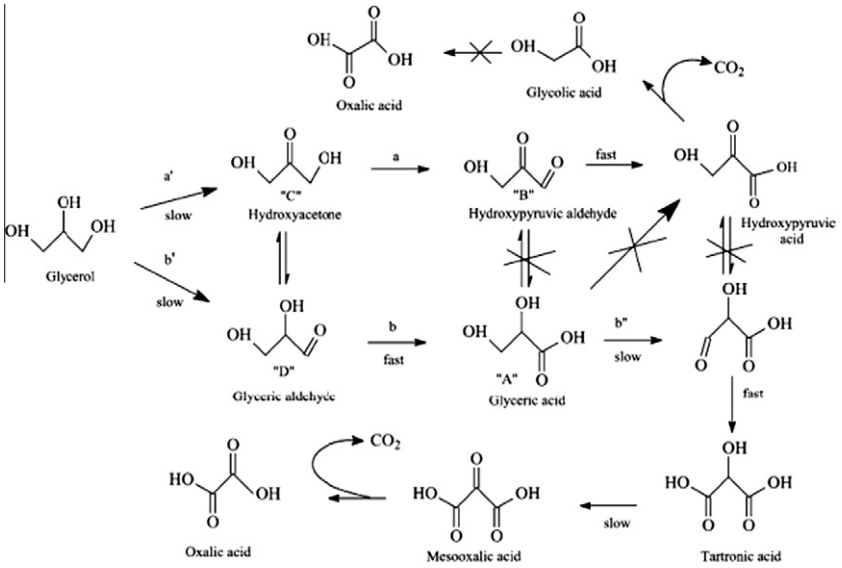

Scheme 1. Reaction pathway for glycerol oxidation.

environmental catalysis and fine chemical production [29]. For catalytic purposes, high surface areas are often desirable. Fortunately over the last few years, spinels have been successfully prepared by different methods, allowing one to obtain materials with tunable surface areas and chemical compositions. Au/$MgAl_2O_4$ appeared promising in gas-phase CO to CO_2 oxidation and in aqueous-phase ethanol oxidation, providing a simple and green route to acetic acid or ethyl acetate [30–32]. Due to the properties of $MgAl_2O_4$ described above, the application of $MgAl_2O_4$ as a catalyst support has been explored.

Here, we investigated the structure and properties of Au nanoparticles, prepared via three different techniques, and supported on $MgAl_2O_4$ spinels that, due to their different properties, could be used to tune the evolution of the glycerol selective oxidation in terms of both activity and selectivity.

2. Experimental

2.1. Materials

Gold of 99.99% purity in sponge from Fluka was used as a gold source for the preparation of $HAuCl_4$ for gold sols. Tetrakis(hydroxymethyl)phosphonium chloride (THPC, 80% solution) from Aldrich was used. NaOH and urea (purity >99%) were from Fluka. Gaseous oxygen from SIAD was 99.99% pure. Glycerol (86–88% solution) from Aldrich was used. Samples of potential reaction products from the oxidation of glycerol were obtained from Fluka and used as standard reference samples for product analysis.

2.2. Support materials

$MgAl_2O_4$ support materials were obtained from Alfa Aesar (commercial) or prepared via flame spray pyrolysis (FP) and coprecipitation for this study (Table 1).

2.2.1. Coprecipitation

The coprecipitation spinel was prepared using a previously reported procedure by dissolving $Al(NO_3)_3{\cdot}9H_2O$ (0.1 M), $Mg(NO_3)_2{\cdot}6H_2O$ (0.08 M) and urea (1.8 M) in distilled water [28]. The pH of the starting solution was adjusted to 2 with nitric acid, and then the solution was heated at 90 °C under magnetic stirring for 24 h. The precipitate was then filtered, washed with distilled water and dried at 100 °C for 16 h. The so-synthesized powder was calcined in air for 1 h at 900 °C.

2.2.2. Flame spray pyrolysis

$Mg(CH_3COO)_2$ and $Al(NO_3)_3{\cdot}9H_2O$ in proper stoichiometric ratio were separately dissolved in propionic and acetic acid, respectively, with 0.2 M overall concentration. The organic solution was fed (4.4 mL/min) to the flame reactor extensively described in previous papers [33–35], together with 5 L/min of oxygen (SIAD, purity >99.95%). The cross-sectional area of the main nozzle was adjusted so to have 1.5 or 0.4 bar as pressure drop through it. Feeding rates to support the ring of flamelets supporting and igniting the central flame were CH_4 = 0.5 L/min and O_2 = 1.0 L/min.

Portions of the prepared $MgAl_2O_3$ powder were further calcined in static air or in flowing oxygen at 450 °C for 4 h.

Table 1
Support characterization of $MgAl_2O_4$ samples.

Support	d_{XRD} (nm)[a]	S_{BET} ($m^2\ g^{-1}$)	Micropore area ($m^2\ g^{-1}$)	Al/Mg[b] (ICP)	Al/Mg[c] (XPS)
Commercial $MgAl_2O_4$	>30	<1	–	–	6.8
Precipitation $MgAl_2O_4$	3.5	176	146	1.4	4.0
Flame pyrolysis $MgAl_2O_4$	18.5	70	12	2.8	3.5

[a] Measured by Sherrer equation at 2θ = 37.
[b] Theoretical Al/Mg = 2 (stoichiometric).
[c] Ratios from Al2s/Mg2p analysis.

2.3. Catalyst preparation

$Au/MgAl_2O_4$ catalysts were prepared using three independent methods: sol immobilization (THPC sol), deposition precipitation (DP), and magnetron sputtering (MS).

2.3.1. From metallic sol (THPC-protected sol)

Gold sols generated in the presence of the THPC/NaOH system were prepared as reported elsewhere [36]. A freshly prepared 0.05 M solution of THPC (0.5 mL) was added to a 10^{-3} M solution of NaOH. After 6 min, 2 mL of $HAuCl_4$ (5.0 mg/mL Au) was added dropwise, yielding a brown metallic sol. Within a few minutes of sol generation, the support was added under vigorous stirring. The amount of support was calculated for having a final gold loading of 3 wt%. After 2 h, the slurry was filtered and the catalyst washed thoroughly with distilled water; it was then used in the wet form. The total Au loading was checked by ICP analysis on the filtered solution using a Jobin Yvon JY24 spectrometer.

2.3.2. Deposition–precipitation with urea

$Au/MgAl_2O_4$ were prepared following the deposition–precipitation method reported by Louis and co-workers using urea as the precipitating agent [37]. The support (1.00 g) was added to 200 mL of an aqueous solution of $HAuCl_4$ (160 mg/L Au) and of urea (0.42 M). The amount of support was calculated for having a nominal gold loading of 3 wt% (10% excess). The suspension, thermostated at 80 °C, was vigorously stirred for 4 h, until pH 7 was reached. The slurry was then filtered, washed thoroughly with water, dried at 80 °C for 2 h and then calcined in air at 450 °C for 4 h. The actual Au loading (reported in Table 2) was calculated by ICP analysis on the filtered solution using a Jobin Yvon JY24 spectrometer.

2.3.3. Magnetron sputtering

A high-purity gold target (99.99% Refining Systems, Las Vegas, Nevada, USA) attached to a magnetron source was sputtered at an applied power of 14 W in an argon plasma for 1.5 or 2 h (Table 2) [38–40]. The sputtered species were deposited onto the support material as it was tumbled in a stainless steel cup rotated at 100 RPM with two 2.54″ Teflon stir bars to promote tumbling of the powders. Time of deposition was varied to control the weight loading and limit the amount of gold deposited so that nanoparticles were formed (Table 2). At the end of the deposition process, some of the support material was stuck to the side of the inner SS cup, while most of the powder was freely tumbling. In order to collect the powder, the inner SS cup was simply removed and inverted onto a piece of weighing paper. The powder that was stuck to the side remained in the cup and was not used for the subsequent work. Gold loading was determined by dissolving the Au from a sample of $Au/MgAl_2O_4$ in 5 mL of freshly prepared aqua regia (3:1 mixture of hydrochloric acid and nitric acid), filtering off the solid, then diluting the wash and analyzing it using a Thermo Jarrell Ash IRIS Inductively Coupled Plasma (ICP) Optical Emission Spectrometer [38–40].

2.4. Materials characterization

X-ray diffraction (XRD) experiments were performed on a Rigaku D III-MAX horizontal-scan powder diffractometer with Cu Kα radiation, equipped with a graphite monochromator in the diffracted beam (Fig. 1). The crystallite size was estimated from peak half width ($2\theta = 37°$) by using the Scherrer equation with corrections for instrumental line broadening ($\beta = 0.9$). Specific surface area (S_{BET}) was measured by N_2 adsorption/desorption at 77 K using a Micromeritics ASAP 2010 apparatus, after outgassing at

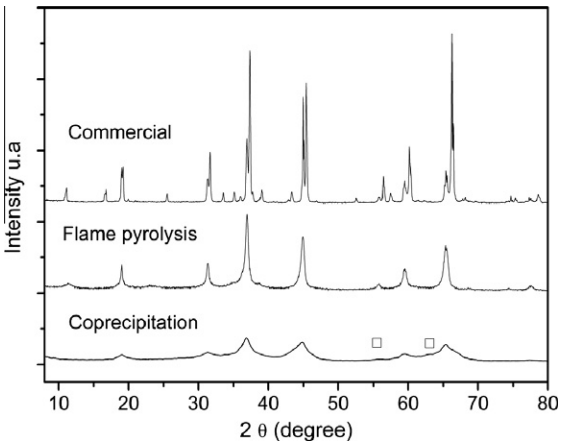

Fig. 1. XRD spectrum of the $MgAl_2O_4$ spinels. MgO peaks are marked (□).

Table 2
STEM, XPS and activity data for $Au/MgAl_2O_4$ samples in glycerol oxidation.

Support	Au wt%	Preparation[c]	STEM (nm)		XPS		Activity mol conv $(Au\ mol)^{-1}\ h^{-1}$[a]	Selectivity[b]				
			Mean size	σ	BE (eV)	Al2s/ Mg2p		GLY	TAR	GLYC	FORM	OXA
Commercial $MgAl_2O_4$	–	bare	–	–	–	6.9	0	nd	nd	nd	nd	nd
	3.0	THPC	13.7	21.2	84.0	11.7	0	nd	nd	nd	nd	nd
	2.7	DP calcined	9.1	6.8	83.6	15.6	120	21	3	72	2	2
	0.3	MS (2 h)	4.1	2.1	83.6	7.0	908	46	6	42	0	6
Coprecipitation $MgAl_2O_4$	–	bare	–	–	–	4.0	0	nd	nd	nd	nd	nd
	3.0	THPC	3.9	2.4	83.6	6.0	1100	55	9	22	10	1
	1.5	DP calcined	2.2	0.4	83.6	4.0	1390	56	14	27	0	3
	0.4	MS (2 h)	2.9	1.3	82.8	4.0	67	54	1	45	0	0
Flame pyrolysis $MgAl_2O_4$	–	bare	–	–	–	3.5	0	nd	nd	nd	nd	nd
	3.0	THPC	4.2	2.6	84.1	4.2	896	63	9	25	0	3
	3.1	DP calcined	3.3	2.2	83.7	6.1	930	61	6	29	1	3
	1.3	MS (1.5 h)	2.9	1.5	83.4	3.6	1080	54	6	34	1	5

[a] Conversion per hour per mol of metal.
[b] Selectivity at 50% conversion. GLY: glycerate; TAR: tartronate; GLYC: glycolate; FORM: formate; OXAL: oxalate.
[c] Sputtering time at 14 W applied power. Reaction conditions: [glycerol] = 0.3 M; NaOH/reactant = 4 mol/mol; reactant/Au = 1000; $p(O_2) = 3$ atm; $T = 50$ °C.

300 °C for at least 6 h. Microporosity was estimated using the t-method.

Al and Mg contents of the support material were estimated by ICP-MS measurements conducted with a Perkin Elmer ELAN 6000 instrument. Samples were digested with concentrated HNO_3 under microwave power then diluted and compared to calibration data obtained for Al and Mg species.

X-ray photoelectron spectroscopy (XPS) measurements were performed with a PHI 3056 spectrometer equipped with an Al anode source operated at 15 kV and an applied power of 350 W and a pass energy of 93.5 eV. Samples were mounted on in foil since the C1s binding energy, from adventitious carbon on the samples, was used to calibrate the binding energy shifts of the sample (C1s = 284.6 eV). The accuracy of binding energies (BE) can be estimated to be ±0.2 eV. Surface composition analysis for the catalysts was complicated by the overlap between Au4f species (photoelectron energy Au4f 7/2 = 84.0 eV; Au4f 5/2 = 88 eV) and the Al2p (photoelectron energy ~75 eV) and Mg2s (photoelectron energy ~88 eV) photoelectron lines (Fig. 2). Therefore, qualitative analysis of the Al:Mg surface chemistry was performed using the Al2s (photoelectron energy ~120 eV) and Mg2p (photoelectron energy ~50 eV) and comparing ratio's of these peaks with and without gold on the surface. It should be stressed these ratios are a guide not absolute concentrations.

Scanning transmission electron microscopy (STEM) images were collected with a Hitachi HD2000 STEM operated at 200 kV. The samples were imaged in the high-angle annular dark-field imaging mode (HAADF). This provides Z-contrast imaging [41], where the image intensity depends on the thickness and approximately the square of the atomic number of the elements. Particle sizes were determined by measuring the widest point on the nanoparticle image to account for particles that may not be orthogonal to the electron beam using the program ImageJ [42].

2.5. Oxidation experiments

The reactions were carried out in a thermostated glass reactor (30 ml), provided with an electronically controlled magnetic stirrer, connected to a 5-L reservoir containing oxygen at 300 kPa. The oxygen uptake was followed by a mass-flow controller connected to a PC through an A/D board, plotting a flow/time diagram. Polyol (0.3 M solution), NaOH (1.2 M solution) and the gold catalyst (polyol/metal = 1000 mol/mol) were mixed in distilled water (total volume 10 ml). The reactor was pressurized at 300 kPa with O_2 and thermostated at 50 °C. Stirring of the reactants began after an equilibration time of 10 min. Samples were taken after 15, 30 and 60 min and analyzed using a Varian 9010 high-pressure liquid chromatograph (HPLC) equipped with a Varian 9050 UV (210 nm) and a Waters R.I. detector in series. A Varian MetaCarb H Plus column (300 × 7.8 mm) was used with aqueous H_3PO_4 0.1% wt/wt (0.4 ml/min) as the eluent. Samples of the reaction mixture (167 µl) were diluted (5 ml) using the eluent. Products were confirmed by comparison with pure products obtained from Fluka.

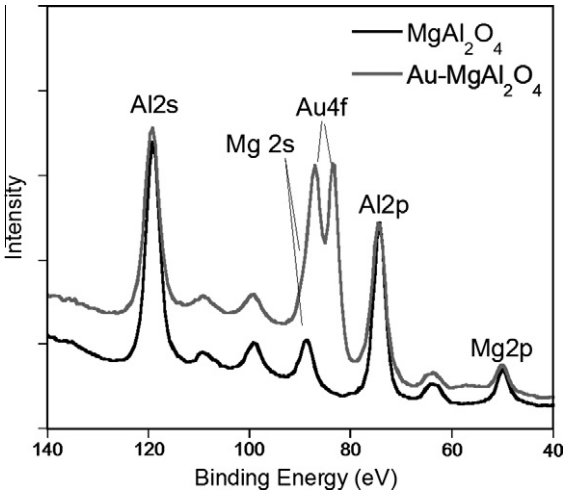

Fig. 2. XPS spectrum showing the Au, Mg, and Al photoelectron lines. Not identified peaks are due to Mg and Al shake-up lines.

3. Results and discussion

3.1. Support characterization

XRD spectra of the samples are reported in Fig. 1. All the three supports exhibited a spinel-type $MgAl_2O_4$ crystalline phase, though crystallite sizes clearly differ as indicated by the width of the peaks. The commercial material has extra diffraction peaks from a secondary oxide phase(s) and is not phase pure. Using the Scherrer formula, crystal size at $2\theta = 37°$ was estimated to be ≫30 nm for the commercial support, 3.5 nm for the spinel obtained by coprecipitation, and 18.5 nm for the material obtained by flame pyrolysis. Two peaks originating from MgO ($2\theta = 56°$ and 64°, Fig. 1) were observed for the spinel obtained by coprecipitation. This MgO is a result of the preparation method [43] where extra Mg^{2+} precursor was used to prevent substoichiometric precipitation of $Mg(OH)_2$.

BET surface areas (S_{BET}, see Table 1) correlated well with the XRD crystal size data: commercial $MgAl_2O_4$ $S_{BET} < 1$ m^2 g^{-1}, coprecipitation $MgAl_2O_4$ $S_{BET} = 176$ m^2 g^{-1}, FP $MgAl_2O_4$ $S_{BET} = 70$ m^2 g^{-1}. For the commercial support, the contribution of microporosity to the total surface area was negligible, whereas for the spinel obtained by coprecipitation and FP, the micropore area was 146 m^2 g^{-1} (83% total surface area) and 12 m^2 g^{-1} (17% total surface area), respectively.

Bulk Al/Mg ratios (determined by ICP analysis) and Al/Mg surface ratios (determined by XPS analysis) varied significantly from the stoichiometrically predicted ratios ($Al/Mg_{THEO} = 2$) depending on the preparation techniques. It should be noted that Al2s and Mg2p peaks were used to analyze the XPS data. The reason for these peaks to be chosen is because the normally used Al2p and Mg2s peaks overlap with the Au4f data (Fig. 2). As discussed above, for the coprecipitation method, a slight excess Mg^{2+} precursor was used to prevent substoichiometric precipitation of $Mg(OH)_2$, according to Wajler et al. [43]. This explains why the observed bulk Al/Mg atomic ratio is lower than theoretical values (1.4 vs. 2) (Table 1). ICP data obtained for the FP support material indicates that the total composition is Al-rich. Unfortunately, bulk ICP data are not available for the commercial $MgAl_2O_4$ as we were unable to completely mineralize this material for ICP measurements.

Surface analysis (XPS) also indicates significant deviations from ideal surface stoichiometry. All the supports show Al-rich surface in the order flame pyrolysis (Al/Mg = 3.5), coprecipitation (Al/Mg = 4.0) and finally commercial spinel (Al/Mg = 6.8), indicating a segregation of species during the synthesis of the support materials (Table 1).

3.2. Catalyst characterization

The catalysts prepared in this study all contained metallic gold clusters as indicated by X-ray photoelectron spectroscopy data which showed gold $4f^{7/2}$ photoelectron binding energies in the range of 84.1–82.8 eV, Table 2. The lower gold binding energies, compared to bulk gold foil (84.0 eV), are consistent with the formation of small metallic gold clusters [44–46] (Fig. 2).

Particle sizes of the deposited gold clusters varied depending on synthesis methodology and support material properties. Representative STEM data collected for the Au/$MgAl_2O_4$ samples are shown in Fig. 3 as well as histograms evaluated on more than 400 gold particles. Mean sizes and standard deviation are reported in Table 2. In general, all the samples investigated for this study appeared uniformly coated with gold nanoparticles with the exception of the THPC-prepared samples which indicated large areas of support material not covered with gold nanoparticles and a higher concentration of large agglomerates. Gold particles preformed in a THPC sol showed the largest average particle size when immobilized on the commercial $MgAl_2O_4$; however, this average is significantly skewed to larger particle sizes due to the formation of several large agglomerates, Fig. 3. It is unlikely the THPC-prepared gold particles were too small to image because the THPC sol prepares gold nanoparticles that are about 2 nm in diameter which is larger than the instrumental resolution of the STEM (<1.0 nm in diameter). A gross evaluation, assuming hemispherical gold particles, allows us to estimate that more than 95% of the total gold is sequestered in the large particles. The particle sizes are consistent with what has been observed for THPC-prepared clusters deposited on higher surface area materials such as active carbon [47].

Gold catalysts prepared by the urea deposition–precipitation process (DP) and magnetron sputtering (MS) were the most uniform from support to support (smallest standard deviation in particle size for all the catalysts observed in this study) with the exception of Au on commercial $MgAl_2O_4$, which are characterized by larger Au particle sizes (9 nm), probably because of the very low surface area of the support which promotes particle aggregation.

Gold cluster formation mechanisms from the three different synthesis procedures are all different. The THPC-prepared clusters were preformed in solution and deposited as clusters on the support material. Total transfer of gold from solution is observed (nominal and actual loading value coincident 3%) but large gold clusters often form due to the high concentration of gold deposited over a limited number growth sites promoting gold agglomeration. In contrast, the DP method produced smaller particles than the THPC method but the efficiency of DP in the deposition of gold (given by gold loaded – initial gold amount in the solution) is a function of nucleation rate and bond strength between the gold precipitate and the support materials surface. Due to this variation, we observe differences in weight loading (theoretical 3.1 wt%) among the three supports reaching a quantitative loading of gold only in the case of the FP $MgAl_2O_4$ (Table 2: FP 3.1 wt%, commercial 2.7 wt%, coprecipitation 1.5 wt%). It should be also noted that the mean size of the DP-prepared catalysts decreased as the surface area increased resulted in a slightly smaller particle size than THPC-prepared samples which were independent of surface area above a certain area. The magnetron sputtering process entails depositing an atomic flux of gold atoms onto the support surface where the atoms nucleate and grow to form catalyst clusters; nanoparticles form because of low interfacial binding energy between the gold and the support and an insufficient concentration of deposited material to create a thin film or coating on the substrate.

At this point, the growth mechanisms and processes that control particle sizes are not well understood, but qualitative trends have been observed. The sputtering process is a line-of-sight technique, so only surfaces directly exposed to the metal flux will capture atoms. Consequently, catalysts are grown in "egg-shell" like configurations on the outside of a support material and not within a support material or in micropores. Gold loading and particle sizes are a function of deposition time, material volume, and exposed surface area [48]. Thus, higher weight loadings at lower deposition time could be obtained for the gold on the $MgAl_2O_4$ support material prepared by flame pyrolysis with respect to coprecipitated one because most of the surface area originates from outside of the materials' grains (Table 1; $S_{microp} - S_{BET}$), and the $MgAl_2O_4$

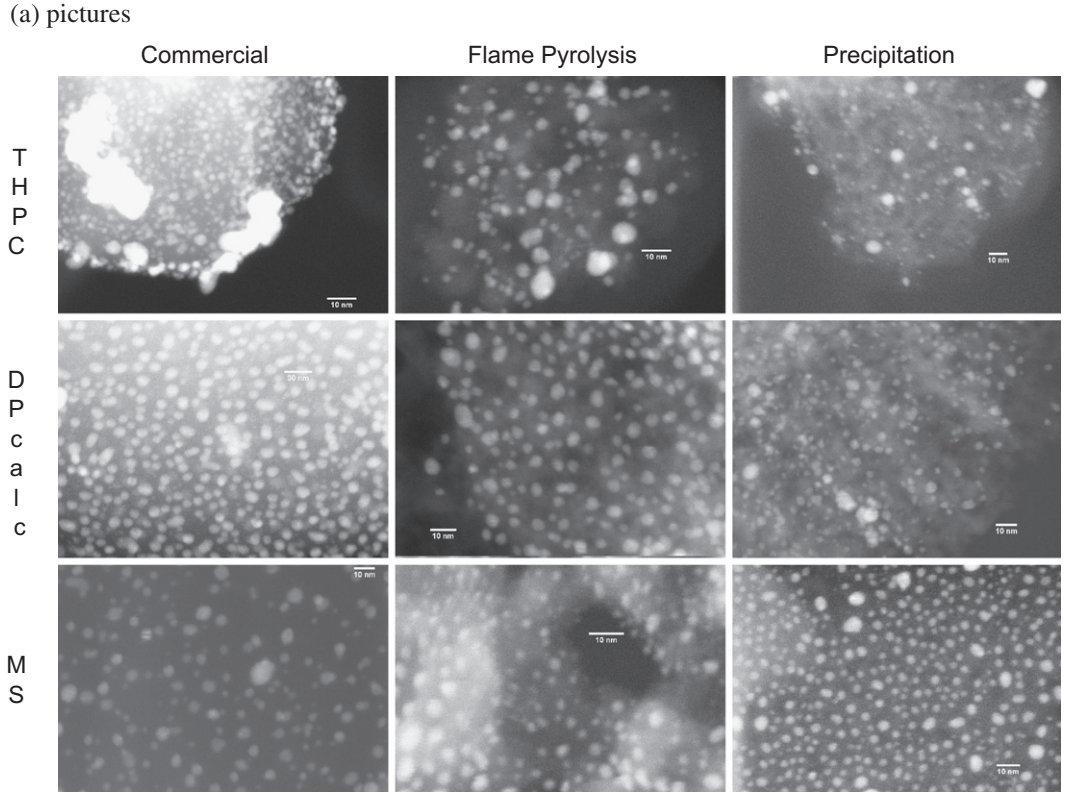

Fig. 3. STEM of the Au/$MgAl_2O_4$ catalysts (a) pictures and (b) histograms.

(b) histograms

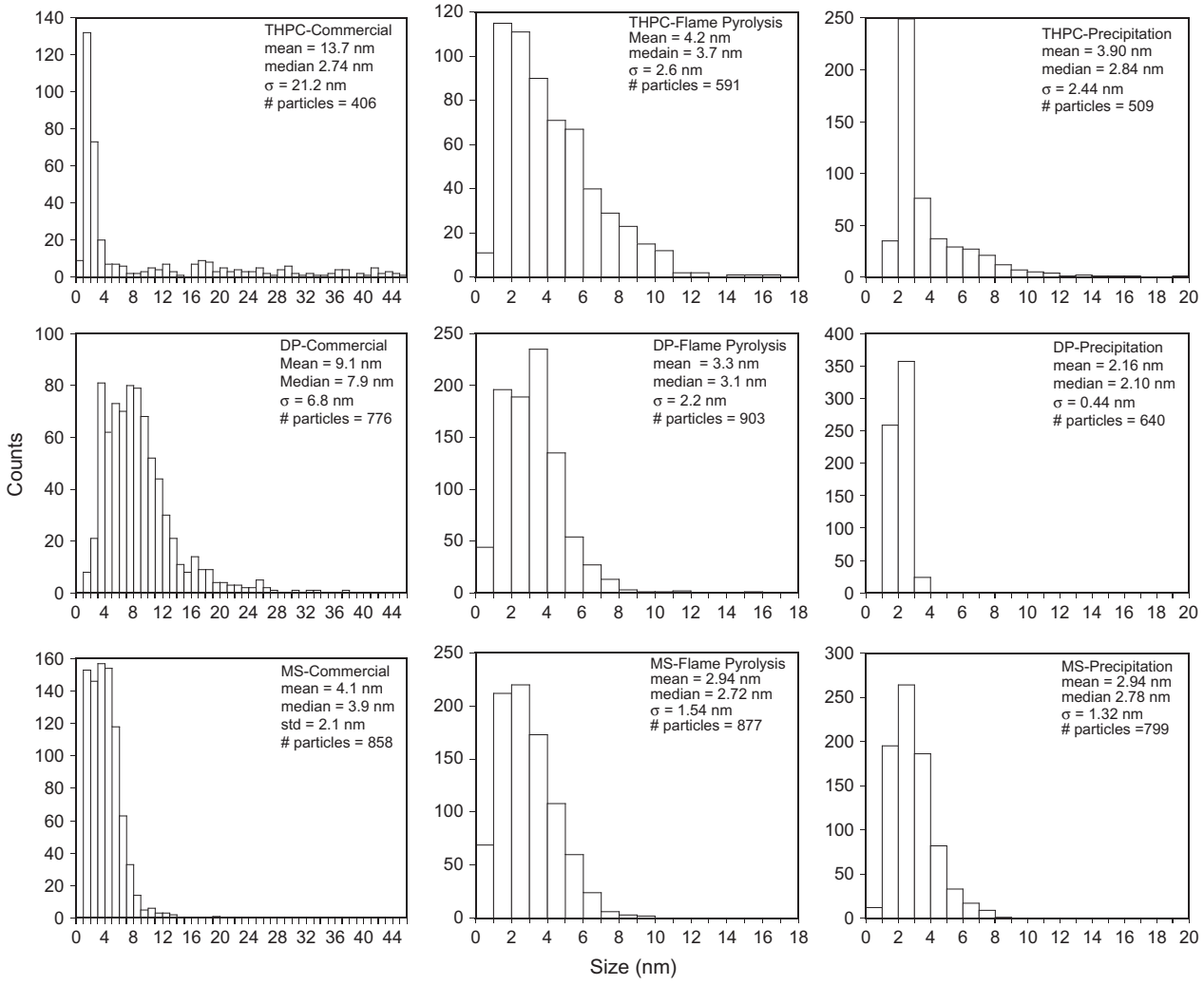

Fig. 3 (*continued*)

prepared by flame pyrolysis has a much lower tamped density (larger volume) effectively resulting in more area for the gold clusters to grow over (Table 1). Commercial spinel presents a very low SA (<1 $m^2\ g^{-1}$) and a low loading of gold as in the case of coprecipitated spinel. Consequently, deposition time is varied to restrict the size of the gold clusters; higher weight loadings can be obtained by increasing the deposition time but resulted in dense gold films evidenced by their gold color and absence of $MgAl_2O_4$ in the XPS spectra, due to burial by gold, and were not explored further. In addition to surface area considerations, the growth of clusters on the surface under these conditions will be highly dependent on the surface chemistry of the support material. Subtle variations in hydroxyl concentration will have a dramatic effect on particle sizes [38]. Thus, a compromise between the loading and particle size had to be chosen (Table 2). A 1.5- to 2-h deposition was adopted for limiting particle growing despite sometime a low Au loading was obtained (Table 2: commercial 0.3 wt%, coprecipitation 0.4 wt%). Sputtered or DP prepare clusters, in contrast to THPC grown clusters, do not present any organic protecting groups on their surface.

XPS characterization of the prepared catalysts revealed insights into the nucleation and growth of clusters prepared via these three techniques. Table 2 reports Al/Mg ratios determined for the gold catalysts. It should be reiterated again that these numbers should be used for a guide since they are comparing the Al2s/Mg2p peaks instead of the typically used Al2p and Mg2s peaks (Fig. 2). THPC and DP preparations generally produce an increase in the Al concentration of the surface (except for the DP-on coprecipitated spinel) versus the native oxide surface. This change in Al/Mg ratio is not due to the selective dissolution of Mg because all preparations occur under basic conditions where Mg compounds are sparingly soluble. Instead, this result indicates that gold in the solution phase preferentially adsorbs on the Mg^{2+} sites during the preparation of the catalyst thus resulting in a shielding of the magnesium in the XPS spectra. This interpretation is consistent with the isoelectric point theory where the Mg sites (IEP MgO ~12) in the pH 7–9 range used for catalyst preparation in this work have a sufficiently positive charge to selectively bind gold precursors (negatively charged as $Au(OH)_x^{n-}$ or Au(0)/THPC) stronger than more neutral Al sites (IEP ~8–9) [49]. In contrast, there was no change in the Al/Mg ratio for the MS-prepared catalysts. This is because the growth mechanism for these catalysts does not rely on the absorption of species to specific sites available in the solution phase; instead, the particles are believed to nucleate at hydroxyl or vacancy sites uniformly dispersed on the oxide [38].

3.3. Glycerol oxidation

To evaluate the correlation between surface chemistry, protecting group, particle size and catalytic activity, we analyzed our materials in the aqueous-phase oxidation of glycerol as this reactant allows us to study activity but also selectivity of our catalytic materials. Experimentally measured catalytic activities (mol of glycerol converted per hour per mol of metal) and selectivities at 50% conversion to various products are listed in Table 2. In general, the activity of the catalysts followed the typical trend where the smaller particles were more active for the oxidation of glycerol, Fig. 4 [11,21,24,50]. As noted above, an increase in the surface area resulted in a decrease in particle sizes. Thus, the DP-prepared catalysts on coprecipitated $MgAl_2O_4$, characterized by smallest particle sizes, were the most active catalysts (Table 2). Fig. 5 shows the reaction profile of this catalyst.

Interestingly, from the selectivity point of view, there are significant deviations compared to trends in selectivity observed for other supported gold catalysts used in the same reaction (glycerol oxidation), namely the selectivity to C3-type products (glycerate and tartronate – Scheme 1) decreases as particle sizes decrease [50]. Evaluating the product distribution when Au on spinels were used as the catalyst (Table 2), we noted that selectivity to C3 products do not follow this trend. For example, Au on Coprec-$MgAl_2O_4$ (mean diameter 3.9(THPC); 2.2(DP); 2.9(MS)) have similar selectivities to glycerate (GLY) products (S50 to GLY between 54% and 56%) (Table 2). This did not surprise us as the particle sizes of metallic nanoparticles are very similar. However, the DP-Commercial catalyst shows as the main product glycolate (selectivity 72% at 50% conversion) deriving from C–C bond cleavage (Scheme 1) instead of the expected enhanced selectivity to C3 products due to quite large Au particles (9.1 nm). Looking at XPS analysis, we noted that a peculiar characteristic of this sample lies on the highest concentration of surface Al (Al/Mg ratio 15.6 – Table 2). Moreover, we also noted that in all the other cases, there is a direct correlation between the surface Al/Mg ratio and the production of glycerate. Fig. 6 shows, in the case of DP-prepared catalyst, the almost linear correlation we found between the Al/Mg ratio revealed by XPS and the selectivity (at 50% conversion) toward glycerate. As shown from Table 2, catalyst with similar particle size (coprecipitated THPC and FP THPC 3.9 and 4.2 nm) but with different Al/Mg ratio (6.0 vs. 4.2) showed a different C3 selectivity (glycerate and tartronate), higher for lower Al/Mg ratio (S50 64%, Al/Mg 6.0 for coprecipitation-THPC vs. S50 72%, Al/Mg 4.2 for FP THPC). Conversely, when the Al/Mg ratio is similar (coprecipitated DP and FP THPC 4.0 and 4.2) but the particle sizes are different (2.2 for CoprecDP vs. 4.2 for FP THPC), the selectivity to C3 (glycerate and tartronate) only slightly increases for larger particle size (72% for FP THPC with 4.2 nm vs. 70% for CoprecDP with 2.2 nm) following the expected trend. We can conclude then that selectivity is correlated with the concentration of surface Al on the support one where the Al-rich material gives the lowest C3 (glycerate and tartronate) product concentration (<25% in best case), and the most Mg-rich support material produces the highest C3 (glycerate and tartronate) product formation (~60–70%) influenced (even slightly) by typical size-mediated selectivity discussed above, Table 2. Note that also in the case of MS-prepared samples, we observed the lowest selectivity toward the C3 (glycerate and tartronate) products (52%) when the commercial spinel was used as the support i.e. the richest Al^{3+} surface (Al/Mg = 7.0) (Table 2). To determine if this trend is a specific characteristic of the type of substrate (glycerol), the Au on Commercial-DP catalyst has been also used in the oxidation of ethylene glycol (Table 3). Also, in this case, we observed the ability of this catalyst in promoting the C–C bond scission. Indeed, a 50% selectivity (at 50% conversion) to formate (HCOONa) was obtained, value to be compared with only a 5% selectivity to formate using Au on coprecipitated-THPC that shows a lower Al/Mg surface ratio (6.0 vs. 15.6) (Table 3).

It has been reported that during the oxidation of glycerol with gold, the C–C bond cleavage could be ascribed to the native H_2O_2

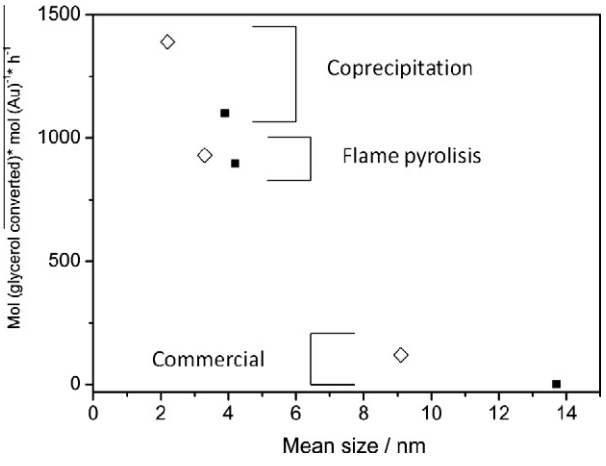

Fig. 4. Activity vs. Au particle size (◇ DP; ■ THPC).

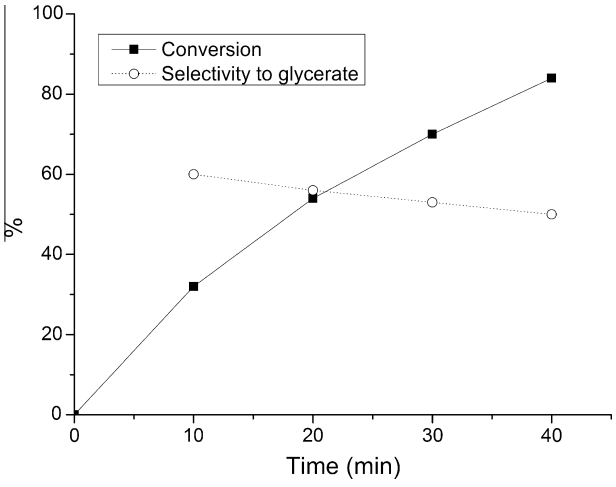

Fig. 5. Reaction profile for DP-Au coprecipitated $MgAl_2O_4$.

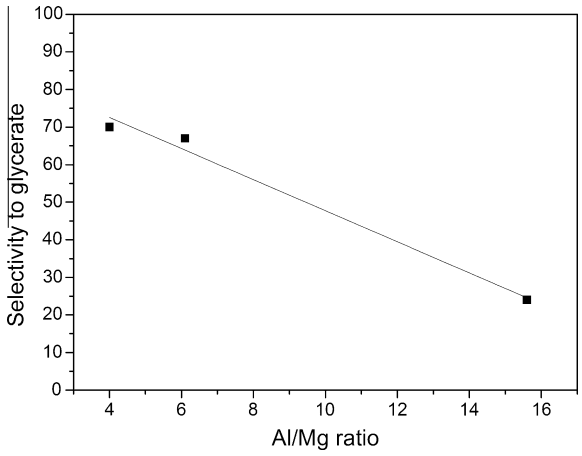

Fig. 6. Correlation between Au/Mg surface ratio and glycerate selectivity at 50% conversion for DP-prepared catalysts.

Table 3
Activity data for $Au/MgAl_2O_4$ samples in ethylene glycol oxidation.

Support	Au wt%	Preparation	XPS	Activity mol (Au mol)$^{-1}$ h^{-1}[a]	Selectivity[b]		
			Al2s/Mg2p		Glycolic acid	Formic acid	Oxalic acid
Commercial $MgAl_2O_4$	2.7%	DP calcined	15.6	80	47	50	3
Coprecipitation $MgAl_2O_4$	3%	THPC	6.0	870	93	5	2

[a] Conversion per hour per mol of metal.
[b] Selectivity at 50% conversion. Reaction conditions: [ethylene glycol] = 0.3 M; NaOH/reactant = 4 mol/mol; reactant/Au = 1000; $p(O_2)$ = 3 atm; T = 50 °C.

Table 4
Literature survey for glycerol oxidation using gold catalysts.

Catalyst	Glycerol/Au	NaOH	Temperature (K)	pO_2 (bar)	Selectivity to glyceric acid (at conversion) (%)	Refs.
1% Au charcoal	538	1	333	3	100 (56)	[9]
1% Au/graphite	538	1	333	3	100 (54)	[9]
Au/AC	500	2	333	1	75 (30)	[11]
1% Au/AC	500	4	303	3	95 (90)	[21]
Au/TiO_2	500	4	323	3	58 (90)	[22]
Au/AC	110,000	2	333	10	82 (48)	[24]
1% Au/AC	500	2	333	10	43 (35)	[25]
1% Au/AC	500	2	333	10	70 (37)	[25]
1% Au/Dowex M-43	1000	4	323	3	60 (90)	[26]
2.7% $Au/MgAl_2O_4$ DP-Commercial	1000	4	323	3	21 (50)	Present work
3.1% $Au/MgAl_2O_4$ DP-FP	1000	4	323	3	61 (50)	Present work

[24,51]. However, in the current cases, we can exclude this type of contribution to C–C bond cleavage as we did not find any relevant difference among all the catalysts (final H_2O_2 concentration <0.2 mM). Thus, the contribution of the H_2O_2-mediated oxidative cleavage, if any, should be similar in all the tests and excluded that the effect on selectivity of the Al-rich surface was correlated to a higher amount of H_2O_2. Most probably, the reason should be found in a different adsorption/desorption rate of intermediates. In fact, it was already found that by increasing the residence time on the catalyst, the C–C bond cleavage amount increased [26].

Using the MS preparation method, a further intriguing trend was obtained. In this case, the Al/Mg ratio is virtually unchanged for all the three catalysts before and after gold deposition (Table 2), even the difference among the three samples is not negligible (Al/Mg ratio 7.0 for commercial, 4.0 for coprecipitated and 3.6 for flame pyrolysis derived spinels). Similar gold particle sizes (2.9 nm) on coprecipitated or FP spinels that show a similar Al/Mg surface ratio (4.0 vs. 3.6) presented a similar selectivity (Au coprecipitation 55% vs. Au FP 60%) but, unexpectedly, a large difference in catalytic activity was obtained (Table 2: MS-FP 1080 converted mol (Au mol)$^{-1}$ h^{-1}, whereas MS Coprec-spinel 67 converted mol (Au mol)$^{-1}$ h^{-1}). The main difference between the two spinels is the different surface area and pore distribution, with the coprecipitated spinel containing more micropores than the FP spinel (Table 1). The atomic% of Au measured by XPS for these samples was determined to be 10.0% for the Au/FP-$MgAl_2O_4$ but only 1.9% for Coprec-$MgAl_2O_4$. Normalizing atomic% Au by factoring in weight loading and external surface area from BET measurements (Table 1) revealed there was 2.7 times more surface gold in the gold catalyst on FP-produced $MgAl_2O_4$. Thus, the higher activity observed for the Au/FP-$MgAl_2O_4$ sample with respect to the Au/Coprec-$MgAl_2O_4$ sample can be explained by a higher exposition of active sites to reactant due to the higher concentration of surface gold species.

4. Conclusions

Gold nanoparticles supported on three spinel-type $MgAl_2O_4$ supports prepared using different routes have been explored in the selective liquid-phase oxidation of glycerol. The increasing of Al/Mg surface ratio by XPS after wet gold deposition revealed that gold selectively deposited onto the more basic Mg sites. On the contrary, the Al/Mg ratio was almost the same as before gold deposition in magnetron sputtered gold catalysts showing that in these cases no preferential adsorption of the gold to Mg or Al sites occurred. The catalytic activity generally followed the expected trend based on particle sizes. However, the activity appeared also tuned by the effective exposure of active sites possibly influenced by surface area. During the glycerol oxidation, it appeared that the selectivity of the reaction was only partially ruled out by the gold particle size, while the main determining factor is the surface Al/Mg ratio, the Al-rich surface promoting the C–C bond. This trend was also observed in vic-diol-type molecule as ethylene glycol.

The selective glycerol oxidation has been explored with a lot of catalytic systems [16–26], the gold-based ones appearing the most selective even not always the most active. A direct comparison among the different catalysts is very difficult as different reaction conditions as well as selectivity at different conversions are reported. In Table 4, we tentatively show the most frequently reported data and in this panorama, the present spinel-based catalysts could be considered the most tunable catalytic systems. Moreover, this represents another clear example of how the gold-catalyzed reaction could be tuned by a different interaction of the AuNPs with the support [52].

Acknowledgments

Authors gratefully acknowledge Fondazione Cariplo for financial support. Microscopy studies at Oak Ridge National Laboratory's Center for Nanophase Materials Sciences were sponsored by the Scientific User Facilities Division, Office of Basic Energy Sciences, US Department of Energy. This research (GMV, KvB) was sponsored by the Materials Sciences and Engineering Division, US Department of Energy under contract with UT-Battelle, LLC.

References

[1] G.C. Bond, D.T. Thompson, Catal. Rev. Sci. Eng. 41 (1999) 319.
[2] A. Corma, H. Garcia, Chem. Soc. Rev. 37 (2008) 2096.

[3] C. Della Pina, E. Falletta, L. Prati, M. Rossi, Chem. Soc. Rev. 37 (2008) 2077.
[4] M. Haruta, T. Kobayashi, H. Sano, N. Yamada, Chem. Lett. 2 (1987) 405.
[5] G. Bond, Gold Bull. 42 (4) (2009) 337.
[6] M. Conte, A.F. Carley, C. Heirene, D.J. Willock, P. Johnston, A.A. Herzing, C.J. Kiely, G.J. Hutchings, J. Catal. 250 (2) (2007) 231.
[7] L. Prati, M. Rossi, J. Catal. 176 (1998) 552.
[8] N. Dimitratos, F. Porta, L. Prati, A. Villa, Catal. Lett. 99 (2005) 181.
[9] S. Carrettin, P. McMorn, P. Johnston, K. Griffin, G.J. Hutchings, Chem. Commun. (2002) 696.
[10] A. Abad, C. Almela, A. Corma, H. Garcia, Tetrahedron 62 (2006) 6666.
[11] S. Demirel-Gülen, M. Lucas, P. Claus, Catal. Today 102–103 (2005) 166.
[12] M. Comotti, C. Della Pina, R. Matarrese, M. Rossi, Angew. Chem. Int. Ed. 43 (2004) 5812.
[13] H. Tsunoyama, H. Sakurai, Y. Negishi, T. Tsukuda, J. Am. Chem. Soc. 127 (2005) 9374.
[14] P.G.N. Mertens, M. Bulut, L.E.M. Gevers, I.F.J. Vankelecom, P.A. Jacobs, D.E. De Vos, Catal. Lett. 102 (2005) 57.
[15] A. Villa, D. Wang, D.S. Su, L. Prati, ChemCatChem 1 (2009) 510.
[16] C.H. Zhou, J.N. Beltramini, Y.X. Fan, G.Q. Lu, Chem. Soc. Rev. 37 (2008) 527.
[17] F. Jérôme, Y. Pouilloux, J. Barrau, ChemSusChem 1 (2008) 586.
[18] A. Corma, S. Iborra, A. Velty, Chem. Rev. 107 (2007) 2411.
[19] H. Kimura, K. Tsuto, T. Wakisaka, Y. Kazumi, Y. Inaya, Appl. Catal. A: Gen. 96 (1993) 217.
[20] R. Garcia, M. Besson, P. Gallezot, Appl. Catal. A: Gen. 127 (1995) 165.
[21] F. Porta, L. Prati, J. Catal. 224 (2004) 397.
[22] N. Dimitratos, A. Villa, C.L. Bianchi, L. Prati, M. Makkee, Appl. Catal. A: Gen. 311 (2006) 185.
[23] S. Demirel, P. Kern, M. Lucas, P. Claus, Catal. Today 122 (2007) 292.
[24] W.C. Ketchie, Y. Fang, M.S. Wong, M. Murayama, R.J. Davis, J. Catal. 250 (2007) 94.
[25] N. Dimitratos, J.A. Lopez-Sanchez, J.M. Anthonykutty, G. Brett, A.F. Carley, R.C. Tiruvalam, A.A. Herzing, C.J. Kiely, D.W. Knight, G.J. Hutchings, Phys. Chem. Chem. Phys. 25 (2009) 4952.
[26] A. Villa, C.E. Chan-Thaw, L. Prati, Appl. Catal. B: Environ. 96 (2010) 541.
[27] M. Sankar, N. Dimitratos, D.W. Knight, A.F. Carley, R. Tiruvalam, C. J. Kiely, D. Thomas, G.J. Hutchings, ChemSusChem, doi: 10.1002/cssc.200900133.
[28] J. Mori, W. Watenabe, M. Yoshimura, Y. Oguchi, T. Kawakami, Am. Ceram. Soc. Bull. 69 (1990) 1172.
[29] O.R. Evans, A.T. Bell, T.D. Tilley, J. Catal. 226 (2004) 292.
[30] W.C. Li, M. Comotti, A.H. Lu, F. Schuth, Chem. Commun. (2006) 1772.
[31] C.H. Christensen, B. Jørgensen, J. Rass-Hansen, K. Egeblad, R. Madsen, S.K. Klitgaard, S.M. Hansen, M.R. Hansen, H.C. Andersen, A. Riisager, Angew. Chem. Int. Ed. 45 (2006) 4648.
[32] B. Jørgensen, S.E. Christiansen, M.L. Dahl Thomsen, C.H. Christensen, J. Catal. 251 (1) (2007) 332.
[33] G.L. Chiarello, I. Rossetti, L. Forni, J. Catal. 236 (2005) 251.
[34] G.L. Chiarello, I. Rossetti, L. Forni, P. Lopinto, G. Migliavacca, Appl. Catal. B: Environ. 72 (2007) 218.
[35] G.L. Chiarello, I. Rossetti, L. Forni, P. Lopinto, G. Migliavacca, Appl. Catal. B: Environ. 72 (2007) 227.
[36] D.G. Duff, A. Baiker, P.P. Edwards, J. Chem. Soc. Chem. Commun. (1993) 96.
[37] R. Zanella, S. Giorgio, C.R. Henry, C. Louis, J. Phys. Chem. 106 (2002) 7634.
[38] G.M. Veith, A.R. Lupini, N.J. Dudney, J. Phys. Chem. C 113 (2009) 269.
[39] G.M. Veith, A.R. Lupini, S.J. Pennycook, G.W. Ownby, N.J. Dudney, J. Catal. 231 (2005) 151.
[40] G.M. Veith, A.R. Lupini, S.J. Pennycook, A. Villa, L. Prati, N.J. Dudney, Catal. Today 122 (2007) 248.
[41] D.B. Williams, C.B. Carter, Transmission Electron Microscopy, A Textbook for Materials Science, Springer, New York, USA, 2009. ISBN: 978-0-387-76500-6.
[42] M.D. Abramoff, P.J. Magelhaes, S.J. Ram, Biophoton. Int. 11 (2004) 36.
[43] A. Wajler, H. Tomaszewski, E. Drożdż-Cieśla, H. Węglarz, Z. Kaszkur, J. Eur. Ceram. Soc. 28 (2008) 2495.
[44] J. Radnik, C. Mohr, P. Claus, Phys. Chem. Chem. Phys. 5 (2003) 172.
[45] M.P. Casaletto, A. Longo, A. Martorana, A. Prestianni, A.M. Venezia, Surf. Interface Anal. 38 (2006) 215.
[46] A. Zwijnenburg, A. Goossens, W.G. Sloof, M.W.J. Crajé, A.M. van der Kraan, L.J. de Jongh, M. Makkee, J.A. Moulijn, J. Phys. Chem. B 106 (2002) 9853.
[47] C. Bianchi, F. Porta, L. Prati, M. Rossi, Top. Catal. 13 (2000) 231.
[48] G.M. Veith, A.R. Lupini, S.J. Pennycook, N.J. Dudney, The use of magnetron sputtering for the production of heterogeneous catalysts, in: E. Gaigneaux, M. Devillers, D.E. De Vos, S. Hermans, P.A. Jacobs, J.A. Martens, P. Ruiz (Eds.), Studies in Surf. Sci. and Catalysis, vol. 162, Elsevier, Amsterdam, 2006, pp. 71–78.
[49] X. Hao, L. Quach, J. Korah, W.A. Spieker1, J.R. Regalbuto, J. Mol. Catal. A: Chem. 219 (2004) 97.
[50] S. Carrettin, P. McMorn, P. Johnston, K. Griffin, C.J. Kiely, G.J. Hutchings, Phys. Chem. Chem. Phys. 5 (2003) 1329.
[51] L. Prati, P. Spontoni, A. Gaiassi, Top. Catal. 52 (2009) 288.
[52] G.C. Bond, C. Louis, D.T. Thompson, in: Catalysis by Gold, Imperial College Press, Singapore, 2006.